Climate-driven processes of hillslope weathering

Jean L. Dixon[1]*, Arjun M. Heimsath[1]*, James Kaste[2]*, and Ronald Amundson[3]*
[1]School of Earth and Space Exploration, Arizona State University, 548 Physical Sciences F-wing, Tempe, Arizona 85287, USA
[2]Department of Geology, College of William and Mary, 217 McGlothlin-Street Hall, Williamsburg, Virginia 23187, USA
[3]Department of Environmental Science, Policy and Management, University of California–Berkeley, 137 Mulford Hall, Berkeley, California 94720, USA

ABSTRACT

Climate controls erosion and weathering on soil-mantled landscapes through diverse processes that have remained difficult to disentangle due to their complex interactions. We quantify denudation, soil and saprolite weathering, and soil transport near the base and crest of the western slope of the Sierra Nevada to examine how large differences in climate affect these processes. Depth profiles of fallout radionuclides and field observations show relative differences in erosion and weathering processes at these two climatically diverse sites, and our data suggest fundamentally different patterns of soil production and transport mechanisms: biotically driven soil transport at low elevation, and surface erosion driven by overland flow at high elevation. Soil production rates from cosmogenic ^{10}Be decrease from 31.3 to 13.6 m/Ma with increasing soil depth at low elevation, but show uncertain depth dependence at the high elevation site. Our data also show a positive correlation between physical erosion and saprolite weathering at both sites. Highly weathered saprolites are overlain by weakly weathered and rapidly eroding soils, while chemically less depleted saprolites are overlain by slowly eroding, more weathered soils. Our data are among the first to quantify the critical role of saprolite weathering in the evolution of actively eroding upland landscapes, and our results provide quantitative constraints on how different climates can shape hillslopes by driving processes of erosion and weathering.

INTRODUCTION

Soils are a dynamic interface between the atmosphere, biosphere, and Earth's surface; chemical and physical processes within soils should therefore express the influence of climate on landscape evolution. Climate directly influences the processes affecting hillslope soils by (1) controlling vegetation and fauna, which physically move and mix soil and influence acidity, and (2) affecting chemical weathering by driving soil temperature and water through-flow rates. The effects of temperature and precipitation on chemical weathering are studied through modeling (e.g., Casey and Sposito, 1992), laboratory experiments (e.g., White and Brantley, 2003), examination of soil and stream solutes (e.g., White and Blum, 1995), and the measurement of immobile elements in soil (e.g., Riebe et al., 2004). Soil transport mechanisms also respond to climate and control rates of erosion and chemical weathering, yet an explicit consideration of the role of individual transport processes has not been widely integrated into denudation and/or weathering analyses of soil-mantled terrain.

Potential links between climate and long-term erosion on nonglaciated landscapes are increasingly being examined (e.g., Riebe et al., 2004), but the relationships remain elusive due to limited field data. Attempts to correlate hillslope response to climate have focused primarily on rates of landscape change, and few have quantified the mechanisms by which climate influences erosion and weathering processes (e.g., von Blanckenburg, 2006). Furthermore, we are aware of no studies that have specifically examined links between climate, saprolite weathering, and erosion. Here we employ a novel combination of established methods to quantify chemical weathering in both the soil and saprolite, and link weathering to rates and processes of downslope soil transport. We quantify soil production rates using the in situ–produced cosmogenic radionuclide (CRN) ^{10}Be, and chemical weathering using bulk chemical analyses of soil, saprolite, and bedrock. In addition, we use field metrics and fallout-derived ^{210}Pb and ^{137}Cs in soil profiles to identify transport processes. These combined methods help reveal the underlying differences in weathering and erosion for two landscapes at the ends of a large climate gradient.

STUDY SITES AND APPROACH

The study sites are the end members of a well-studied climosequence along the western slope of the Sierra Nevada range in California (United States). Previous work focused on general trends in soil formation and rates of carbon cycling along the climate gradient (Dahlgren et al., 1997; Trumbore et al., 1996). In this study, a low-elevation grassland site (Blasingame, BG; ~220 m) and a sparsely vegetated, high-elevation subalpine site near the Sierran crest (Whitebark, WB; ~2990 m) are separated by ~2900 m in elevation and 64 km (Fig. 1). Both sites are underlain by unglaciated granodiorite of similar composition (Bateman and Lockwood, 1970, 1976). Annual precipitation increases from 37 to 106 cm and average temperature decreases from 16.6 to 3.9 °C with elevation (Prism database; PRISM Climate Group, 2008). Helium thermochronometry (e.g., Clark et al., 2005) and CRN-dated cave sediments (Stock et al., 2005) suggest that rapid river incision in the Sierra Nevada is likely associated with Cenozoic uplift; however, much of the upland soil mantled-landscape has not responded to this forcing (e.g., Clark et al., 2005). We chose sites with minimal differences in lithology, tectonics, and recent glaciation to isolate the role of climate on erosion and weathering processes in the region, and use the end members along the transect to take advantage of the maximum available climate signal.

We sampled saprolite beneath soil at selected hillslopes, along downslope transects from crest to swale, and measured ^{10}Be in saprolite to determine soil production rates (P_{soil}) (e.g., Heimsath et al., 2005). We measured zirconium concentrations in soil, saprolite, and rock using pressed pellet X-ray fluorescence, and calculated fractional chemical losses in soil and saprolite using the chemical depletion fraction (CDF) (Riebe et al., 2004). We calculated the CDF_{total} (relative dissolved mass loss of soil relative to bedrock), $CDF_{saprolite}$ (from [Zr] in saprolite relative to rock) and CDF_{soil} (from [Zr] in soil relative to saprolite). The sites examined have divergent planform topography, which lacks the complication of an upslope contribution of previously weathered material (Yoo et al., 2007). Thus, in these settings, the CDF largely reflects chemical weathering during soil production. Chemical weathering rates of soils (W_{soil}) and saprolites ($W_{saprolite}$), and physical erosion rates were determined by coupling the CDF with CRN-derived denudation rates (e.g., Riebe et al., 2004) (see GSA Data Repository[1] for equations and derivations).

We examined soil mixing and transport processes using fallout radionuclides and by observations of biological activity in the field. We mea-

*E-mails: jean.dixon@asu.edu; arjun.heimsath@asu.edu; jmkaste@wm.edu; earthy@nature.berkeley.edu (Amundson).

[1]GSA Data Repository item 2009248, nuclide activity data and modeled diffusion coefficients, is available online at www.geosociety.org/pubs/ft2009.htm, or on request from editing@geosociety.org or Documents Secretary, GSA, P.O. Box 9140, Boulder, CO 80301, USA.

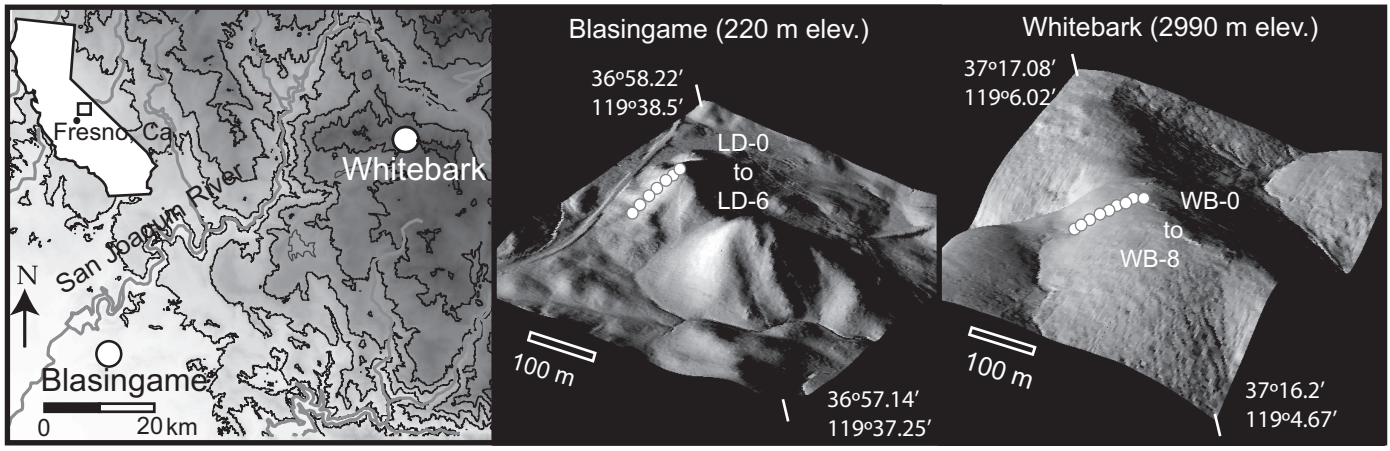

Figure 1. Location of field area showing low-elevation grassland site, Blasingame, and high-elevation subalpine site, Whitebark. Light ranging and detection data (provided by National Center for Airborne Laser Mapping) were used to derive slope and curvature and produce shaded relief images.

sured $^{210}Pb_{excess}$ (shortened here to ^{210}Pb) and ^{137}Cs nuclide activities with depth and calculated total inventories to gain insight into mixing (e.g., Kaste et al., 2007) and soil erosion mechanisms (e.g., Wallbrink and Murray, 1993; Kaste et al., 2006). The nuclide profile depth was defined as the soil depth at which >95% of the cumulative nuclide activity, or inventory, was obtained. We used nuclide profiles to determine the degree of physical mixing, and calculated a diffusion coefficient by the best-fit exponential curve to an advection-diffusion equation (Kaste et al. 2007) (see the Data Repository and Fig. 2 for equations).

We determined the average fractional vegetative cover from photos to estimate soil exposure to raindrop splash and resistance to overland flow. Gopher and ground squirrel burrowing activity at each site was measured by recording burrow number and size at the ground surface within a 2 m swath extending 54–114 m along three contour parallel transects and one profile transect. We calculated a surface area expression of burrowing activity per hillslope area by multiplying burrow density by burrow diameter (see the Data Repository).

PATTERNS OF EROSION AND CHEMICAL WEATHERING

Hillslope soil production rates average 82 ± 10 t/km^2/a (37 ± 4 m/Ma; mean ± standard error) at the low-elevation BG site and 52 ± 5 t/km^2/a (24 ± 2 m/Ma) at the high-elevation WB site. At BG, soil production rates decrease with increasing soil thickness (Fig. 2A) and distance from the slope crest (Fig. 2B), as observed in other temperate landscapes (e.g., Heimsath et al., 2005). This relationship is not shown at WB.

Chemical weathering results in an average net loss of 24% ± 4% of the soil mass at both sites, calculated as the average CDF_{soil}, and CDF values are not significantly different at the two sites. Dahlgren et al. (1997) observed that the clay content of the low-elevation soils exceeds that of WB soils by a factor of two. This suggests a discrepancy in how soil weathering intensity is recorded by CDF and clay abundance. The CDF quantifies net elemental losses; however, secondary mineral formation is the balance between chemical dissolution of primary minerals and the leaching of weathering products. Potential mass loss may exceed net mass loss at low elevation, due to secondary mineral development and retention, in agreement with previous observations of the low leaching potential of clay minerals in these soils compared to high-elevation soils (Dahlgren et al., 1997). Thus, the total chemical alteration at the BG site is greater despite similar net losses to the WB site.

At both sites, CDF_{sap} data indicate that saprolite weathering is a large portion of the total weathering losses, averaging 31% ± 4% and reaching values as high as 56% of the original rock mass. Saprolite weathering rates average 46 ± 13 t/km^2/a at BG and 25 ± 5 t/km^2/a at WB. Physical erosion rates at low and high elevations average 64 ± 12 t/km^2/a and 38 ± 4 t/km^2/a, respectively. At BG, soil chemical weathering rates decline

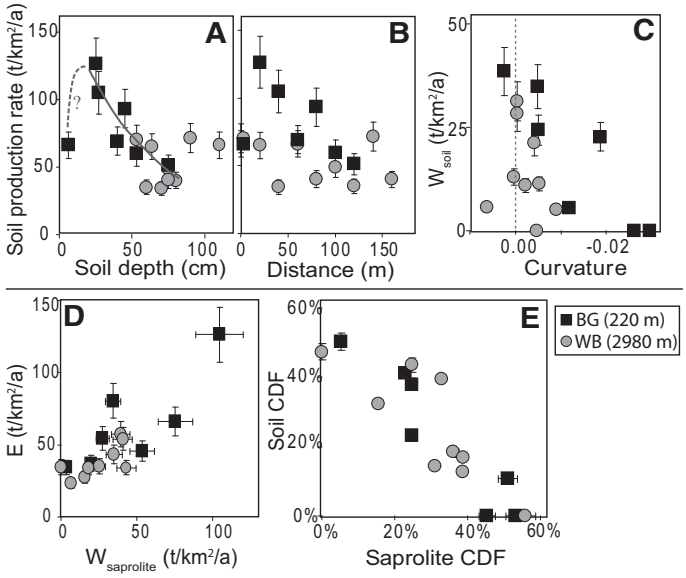

Figure 2. Average ^{10}Be-derived soil production rates (P_{soil}) are higher at Blasingame (BG) than Whitebark (WB) (one-tailed *t*-test, $t = 7.28$, $p = 0.02$). A: At BG, these rates decrease with soil thickness ($P_{soil} = 77e^{-0.017h}$, $r^2 = 0.81$). B: At BG, these rates decrease with distance from crest ($r^2 = 0.81$, $p < 0.01$). Hill crest alone deviates from these trends, suggesting either exponential soil production function with hill crest held up by slower eroding feature such as emergent tor, or humped production function, whereby production rates peak at some finite soil thickness. C: Soil chemical weathering rates (W_{soil}) decrease with increasing convexity (negative curvature) at BG ($r^2 = 0.75$, $p = 0.05$), and insignificantly at WB ($r^2 = 0.31$, $p = 0.19$). D: Physical erosion rates increase with chemical weathering rate of saprolite ($W_{saprolite}$) at both sites (all data: $r^2 = 0.68$, $p = 0.02$; BG: $r^2 = 0.48$, $p = 0.04$; WB: $r^2 = 0.69$, $p < 0.01$). Average rates of erosion are faster at warmer and drier BG (one-tailed *t*-test, $p = 0.04$), compared to colder and wetter WB, although saprolite weathering rates are not significantly different ($p = 0.13$). E: Soil and saprolite weathering extents, shown by chemical depletion fractions (CDF), are negatively correlated (all data: $r^2 = 0.78$, $p < 0.01$; BG: $r^2 = 0.87$, $p < 0.01$; WB: $r^2 = 0.69$, $p < 0.01$).

with increasing convexity (Fig. 2C). Furthermore, physical erosion and saprolite weathering rates at both sites are positively correlated (Fig. 2D), and a strong negative relationship exists between the chemical weathering extents of soils and saprolites (Fig. 2E). We explore implications of these data following the quantification of transport processes.

SEDIMENT TRANSPORT PROCESSES

Fallout radionuclide activity-depth profiles and field observations reveal distinct differences in sediment transport processes at the climate end members. Vegetative density is lowest at the high-elevation WB site, with an average of 83% bare soil versus 4% at the BG site. Low vegetative cover and high precipitation at WB result in low soil resistance to surface water flow and raindrop splash (e.g., Prosser and Dietrich, 1995). Rills began ~40 m downslope from the crest at WB. These have an upslope spacing of 23 m decreasing to an average spacing of 9 m at ~60 m from the slope crest. No rilling was evident at BG. At both sites, bioturbation is evident in soils, and gopher burrows were observed parallel to the ground surface and as deep as the soil-saprolite interface. Mapping gopher burrow density indicates that the burrowing activity at WB is 53% that of BG (Table DR6 in the Data Repository).

Penetration depths of ^{210}Pb and ^{137}Cs increase linearly with burrowing activity at both sites (Fig. 3A), suggesting that bioturbation (through physical transport and altered hydrology) redistributes nuclides to depth in the soil. Assuming that nuclide profiles form primarily by diffusion-like processes, the average diffusive mixing coefficient of soils is 0.28 ± 0.05 cm^2/a at BG, greater than the average 0.15 ± 0.02 cm^2/a at WB (Fig. 2B). The ^{210}Pb inventories do not vary consistently with topography at BG; however, at WB, inventories are lowest where slopes are steepest and have the greatest upslope contributing area (Figs. 3C and 3D). Upslope contributing area has the strongest negative correlation with nuclide inventory at WB, suggesting that soil loss scales with discharge (e.g., Kaste et al., 2006). This correlation, in agreement with the observation of rills, shows that overland flow plays an important role in soil transport at WB.

While overland flow may play a dominant role in sediment transport at WB, it likely has little impact on soil production. Spatial patterns of soil production are distinctly different at these sites (Figs. 2A and 2B), and an apparent soil production function at low elevation is consistent with production mechanisms such as rooting and bioturbation, which are expected to be depth dependent (e.g., Gabet et al., 2003). It is possible that the absence of a trend between P_{soil} and depth at WB (Fig. 2A) is due to soil depths temporarily out of local steady state, and the two deepest samples are anomalies in the sampled transect (see the Data Repository and Fig. DR2). More likely, the absence of depth-dependent soil production at WB (Fig. 2A) and the differences in hillslope patterns of erosion and weathering (Figs. 2B and 2C) suggest that a different mechanism is dominant at the high-elevation site. With average annual temperatures of 3.9 ºC, freeze-thaw may occur at WB; however, this process is also likely depth dependent (e.g., Anderson, 2002). Furthermore, freeze-thaw are likely not dominant soil production or transport processes, given that rills are prominent on the land surface and that soil thicknesses are typically >1 m. Biotite hydration and oxidation may occur at depth in saturated soils during spring snowmelt; however, our data do not speak directly to this mechanism and further research is needed to explain what processes ultimately create these thick high-elevation soils.

MECHANISTIC CONTROLS ON WEATHERING AND EROSION

Chemical weathering facilitates physical erosion by the dissolution of primary minerals, reducing the competence of rock and increasing erodability. Our data are among the first to quantify links between saprolite weathering and physical erosion. Physical erosion rates increase with saprolite weathering rates (Fig. 2D). These data suggest that physical erosion is dependent on the chemical weathering extent and rate of bedrock, because weathered saprolite is more easily detachable and mobilized into the overlying soil column. Furthermore, soil chemical weathering rates at low elevation decline with increasing convexity (Fig. 2C), and the intensities of chemical weathering in soils and saprolites are inversely related (Fig. 2E). Soil weathering may be low where saprolite weathering is high due to faster erosion that reduces soil residence times (e.g., Anderson et al., 2002). As water and sediment are shed off divergent areas of the landscape, decreased water-soil interaction could further result in decreased chemical weathering of soils. Conversely, similar CDF_{total} across the Sierras may support the idea that weathering of parent bedrock is limited by the supply of fresh minerals, rather than reaction rates (e.g., Riebe et al., 2001; West et al., 2005). Saprolite weathering in the Sierras, indicated by saprolite CDFs and rates, is controlled by processes not clearly identified from our study, but is possibly linked to climate, moisture availability, and hillslope morphology. Our data suggest that soil weathering is limited by the availability of fresh minerals, and is therefore low when saprolite has previously depleted this supply.

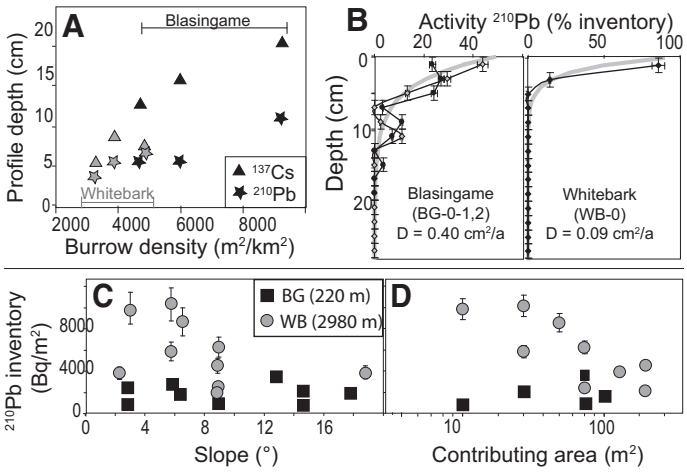

Figure 3. A: Surface burrowing activities from three transects at Blasingame (BG) and Whitebark (WB) increase with associated profile depths for fallout nuclide $^{210}Pb_{excess}$ ($r^2 = 0.95$, $p < 0.01$) and ^{137}Cs ($r^2 = 0.85$, $p < 0.01$). Profile depth is defined as soil depth at 95% cumulative nuclide inventory. B: Fallout profiles show nuclide activity versus depth for hill crests at BG (two profiles shown are 2 m apart) and WB (one profile) and are deeper at BG. We calculated diffusion-like mixing coefficients (D) for each profile (shown by broad gray line) by best fit to the diffusion equation: $a(z) = a_0 * \exp\left[\frac{V - \sqrt{V^2 + 4\lambda D}}{2D}(z)\right]$, where $a(z)$ and a_0 are nuclide activity at depth (z) and surface, respectively, and λ is nuclide decay. Here, we assume that advection velocity (V) is zero. Diffusive mixing coefficients of hill crests are shown, and average hillslope values at each site are 0.28 ± 0.05 cm^2/a at BG and 0.15 ± 0.02 cm^2/a at WB. Also shown are inventories of $^{210}Pb_{excess}$ and ^{137}Cs for downslope soils at low-elevation BG site (gray squares) and high-elevation WB site (black circles). Inventory data points reflect those calculated from individual soil profiles, and activities of additional bulk soil samples gathered downslope. C: Nuclide inventories at high elevation are lower at high slopes; however, no statistically significant correlation exists. D: At BG, inventories do not change markedly, while at WB, nuclide inventories decrease with distances downslope and increasing contributing area ($r^2 = 0.63$, $p = 0.01$). Symbols contain error if not otherwise labeled. Nuclide activities were measured using gamma-ray spectrometry on a broad energy germanium detector at Dartmouth College (Hanover, New Hampshire). Downslope profiles of $^{210}Pb_{excess}$ for each pit, including modeled mixing coefficients, are provided in Data Repository (see footnote 1).

CONCLUSION

We explored the expression of climate on two diverse landscapes by explicitly quantifying the processes and rates of hillslope erosion and weathering. Two principal findings emerge from our data. First, we quantified different rates and processes of soil transport and production at the two sites considered to be end members of a well-studied climosequence. Rates of soil production, erosion, and chemical weathering in saprolite are nearly two times higher at the low-elevation site than at the cooler subalpine site. Measurements of diffusive soil mixing suggest that bioturbation may be twice as important at BG than WB, in agreement with gopher burrow densities. Soil production rates decrease with soil thickness in this vegetated low-elevation site (Fig. 2A), as observed at similar bioturbated grassland landscapes (e.g., Heimsath et al., 2005). At WB, exposed soil, sparse vegetative cover, the presence of rills, and nuclide inventories that increase with contributing area (Fig. 3C) indicate the importance of advective soil transport processes such as overland flow. These results quantify how different climates shape landscapes by influencing the rates and patterns of chemical weathering and soil transport processes.

Second, and perhaps most important, our data show strong feedbacks between physical erosion and chemical weathering at both study sites, despite broad differences between the climates and the soil production and transport mechanisms. Others have reported positive correlations between soil chemical weathering and erosion and have suggested that physical erosion sets the pace of chemical weathering (e.g., Riebe et al., 2004) in soil-mantled terrain. Our data indicate that saprolite weathering and erosion are positively linked (Fig. 2D), and soil weathering is reduced where both saprolite weathering (Fig. 2E) and landscape convexity (Fig. 2C) are high. In summary, our data suggest that saprolite weathering controls erosion and weathering of the overlying soil by depleting primary minerals, decreasing rock competence, and increasing the mobility of weathered material. Because chemical weathering of the saprolite accounts for such significant mass loss from these landscapes, we suggest that not accounting for it leads to missing a critical aspect of erosion-weathering feedbacks.

ACKNOWLEDGMENTS

This work was funded by a National Science Foundation EAR CAREER grant (Heimsath), Sigma Xi Grants in Aid of Research, and the Dartmouth College Department of Earth Sciences. Light ranging and detection data were provided by the National Center for Airborne Laser Mapping. B. Burke, A. Bowling, and L. Hester provided assistance in the field and laboratory. Tim Allen at Keene State University helped with X-ray fluorescence analyses. We thank M. Blasingame and K. Lowe for field support and access to their property. This manuscript benefited greatly from helpful and insightful comments by D.R. Montgomery, R.S. Anderson, G.E. Hilley, and an anonymous reviewer.

REFERENCES CITED

Anderson, R.S., 2002, Modeling the tor-dotted crests, bedrock edges, and parabolic profiles of high alpine surfaces of the Wind River Range, Wyoming: Geomorphology, v. 46, p. 35–58, doi: 10.1016/S0169-555X(02)00053-3.

Anderson, S., Dietrich, W., and Brimhall, G., Jr., 2002, Weathering profiles, mass balance analysis, and rates of solute loss: Linkages between weathering and erosion in a small, steep catchment: Geological Society of America Bulletin, v. 114, p. 1143–1158, doi: 10.1130/0016-7606(2002)114<1143:WPMBAA>2.0.CO;2.

Bateman, P.C., and Lockwood, J.P., 1970, Kaiser Peak Quadrangle, central Sierra Nevada, California—Analytic data: U.S. Geological Survey Professional Paper 644-C, 15 p.

Bateman, P.C., and Lockwood, J.P., 1976, Shaver Lake quadrangle, west-central Sierra Nevada, California—Analytic data: U.S. Geological Survey Professional Paper 774-D, 20 p.

Casey, W.H., and Sposito, G., 1992, On the temperature-dependence of mineral dissolution rates: Geochimica et Cosmochimica Acta, v. 56, p. 3825–3830, doi: 10.1016/0016-7037(92)90173-G.

Clark, M.K., Maheo, G., Saleeby, J., and Farley, K.A., 2005, The non-equilibrium landscape of the southern Sierra Nevada, California: GSA Today, v. 15, p. 4–10, doi: 10.1130/1052-5173(2005)015[4:TNLOTS]2.0.CO;2.

Dahlgren, R.A., Boettinger, J.L., Huntington, G.L., and Amundson, R.G., 1997, Soil development along an elevational transect in the western Sierra Nevada, California: Geoderma, v. 78, p. 207–236, doi: 10.1016/S0016-7061(97)00034-7.

Gabet, E.J., Reichman, O.J., and Seabloom, E.W., 2003, The effects of bioturbation on soil processes and sediment transport: Annual Review of Earth and Planetary Sciences, v. 31, p. 249–273, doi: 10.1146/annurev.earth.31.100901.141314.

Heimsath, A.M., Furbish, D.J., and Dietrich, W.E., 2005, The illusion of diffusion: Field evidence for depth-dependent sediment transport: Geology, v. 33, p. 949–952, doi: 10.1130/G21868.1.

Kaste, J.M., Heimsath, A.M., and Hohmann, M., 2006, Quantifying sediment transport across an undisturbed prairie landscape using cesium-137 and high resolution topography: Geomorphology, v. 76, p. 430–440, doi: 10.1016/j.geomorph.2005.12.007.

Kaste, J.M., Heimsath, A.M., and Bostick, B.C., 2007, Short-term soil mixing quantified with fallout radionuclides: Geology, v. 35, p. 243–246, doi: 10.1130/G23355A.1.

PRISM Climate Group, 2008, Prism database: PRISM Climate Group, Oregon State University, created 5 March 2008, http:// prism.oregonstate.edu.

Prosser, I.P., and Dietrich, W.E., 1995, Field experiments on erosion by overland-flow and their implication for a digital terrain model of channel initiation: Water Resources Research, v. 31, p. 2867–2876, doi: 10.1029/95WR02218.

Riebe, C.S., Kirchner, J.W., Granger, D.E., and Finkel, R.C., 2001, Strong tectonic and weak climate control of long-term chemical weathering rates: Geology, v. 29, p. 511–514, doi: 10.1130/0091–7613(2001)029<0511:STAWCC>2.0.CO;2.

Riebe, C.S., Kirchner, J.W., and Finkel, R.C., 2004, Erosional and climatic effects on long-term chemical weathering rates in granitic landscapes spanning diverse climate regimes: Earth and Planetary Science Letters, v. 224, p. 547–562, doi: 10.1016/j.epsl.2004.05.019.

Stock, G.M., Anderson, R.S., and Finkel, R.C., 2005, Rates of erosion and topographic evolution of the Sierra Nevada, California, inferred from cosmogenic ^{26}Al and ^{10}Be concentrations: Earth Surface Processes and Landforms, v. 30, p. 985–1006, doi: 10.1002/esp.1258.

Trumbore, S.E., Chadwick, O.A., and Amundson, R., 1996, Rapid exchange between soil carbon and atmospheric carbon dioxide driven by temperature change: Science, v. 272, p. 393–396, doi: 10.1126/science.272.5260.393.

von Blanckenburg, F., 2006, The control mechanisms of erosion and weathering at basin scale from cosmogenic nuclides in river sediment: Earth and Planetary Science Letters, v. 242, p. 224–239, doi: 10.1016/j.epsl.2005.11.017.

Wallbrink, P.J., and Murray, A.S., 1993, Use of fallout radionuclides as indicators of erosion processes: Hydrological Processes, v. 7, p. 297–304, doi: 10.1002/hyp.3360070307.

West, J.A., Galy, A., and Bickle, M., 2005, Tectonic and climatic controls on silicate weathering: Earth and Planetary Science Letters, v. 235, p. 211–228, doi: 10.1016/j.epsl.2005.03.020.

White, A.F., and Blum, A.E., 1995, Effects of climate on chemical weathering in watersheds: Geochimica et Cosmochimica Acta, v. 59, p. 1729–1747, doi: 10.1016/0016-7037(95)00078-E.

White, A.F., and Brantley, S.L., 2003, The effect of time on the weathering of silicate minerals: Why do weathering rates differ in the laboratory and field?: Chemical Geology, v. 202, p. 479–506, doi: 10.1016/j.chemgeo.2003.03.001.

Yoo, K., Amundson, R., Heimsath, A.M., Dietrich, W.E., and Brimhall, G.H., 2007, Integration of geochemical mass balance with sediment transport to calculate rates of soil chemical weathering and transport on hillslopes: Journal of Geophysical Research, v. 112, F02013, doi: 10.1029/2005JF000402.

Manuscript received 19 January 2009
Revised manuscript received 9 June 2009
Manuscript accepted 9 June 2009

Printed in USA

1. Study Sites

In the unglaciated upland landscape of the southern Sierra Nevada Range, we chose sites at low (~220 m) and high elevations (~2990 m) that were soil mantled, displayed similar average gradients (Table DR 2), and were underlain by similar granitic rocks. The high elevation site, Whitebark (WB), is located 2 km from Kaiser Pass within a subalpine Canadian vegetative zone. Traveling NE from Fresno, the mountains at Kaiser Pass are the first expression of the Sierra Crest in this region, which then drops to less than 2000 m elevation before rising again to around 4000 m in the bedrock dominated region west of Owens Valley. The low elevation site, Blasingame (BG), in the oak grassland vegetative zone, is located southeast of Millerton Lake, approximately 30 km from Fresno, CA.

At each site, soil pits were excavated every 20 meters along downslope transects. Soil exposures displayed clear boundaries between soils and the saprolite layer, and at both BG and WB gopher burrows had disturbed the soil/saprolite boundary (Figure DR 1). We dug beneath the soil/saprolite boundary to accurately characterize local soil thickness and to collect saprolite for chemical analyses. Figure DR 2 shows downslope topographic profiles and the variation of soil thickness along the two sampled hillslopes. Soil depth at BG increases from 6 to 75 cm with increasing distance from the hillcrest. Soil depths at WB do not vary systematically downslope, however the variation shown in Figure DR 2 suggests the potential for roughly uniform soil thickness or slightly increasing thicknesses downslope at this site. We note that the lack of a clear soil production function (decreasing soil production rate with increasing soil thickness) at WB in Figure 2B of the manuscript is due to three data points, and that Figure DR 2 suggests soil thicknesses at these same sample locations may not be at steady state.

Hillslopes at the two sites are low gradient <20deg and show evidence of gopher burrowing within soil pits and at the ground surface. Burrow holes exposed at the surface lead to transit channels that are between 15-150 cm deep. The BG hillslopes selected for this study have thick grass cover with patchy blue oak cover. Outcropping rock makes up <5% the land surface. Based on field observations, gopher burrowing appears to be the dominant soil transport mechanism active at BG (e.g., Black and Montgomery, 1991). The WB hillslope selected here is sparsely vegetated and small Conifers dot the landscape. Outcropping tors cover <10% of the landsurface and shallow rills (~1/2 m deep) run downslope with an average spacing between 10 and 20m.

2. Measuring Soil Production Rates from Cosmogenic ^{10}Be

We sampled the top-most 2 cm layer of saprolite immediately beneath soil. These samples were processed at Dartmouth College to isolate the beryllium fraction in quartz, following methods outlined by Heimsath et al. (Heimsath et al., 1999). Samples were spiked with a known concentration of ^{9}Be, and the ratio of ^{10}Be:^{9}Be was measured by Accelerator Mass Spectrometry at Lawrence Livermore and Purdue Laboratories to determine the concentration of in-situ produced ^{10}Be. We calculated surface denudation rates, or soil production rates assuming local steady state soil thickness, following methods of Balco et al. (2008), and applying a topographic and soil-depth corrections for spallogenic nuclide production. In-situ ^{10}Be concentrations and derived soil production rates are provided in Table DR 1.

3. Determining Physical Erosion and Chemical Weathering Rates

Theoretical Framework and Equations

Changes in soil mass, expressed as the product of soil density (ρ_{soil}) and soil thickness (h), reflects the balance between soil production (P_{soil}), erosion (E) and weathering (W_{soil}), such that:

$$\rho_{soil}\frac{\partial h}{\partial t} = P_{soil} - E - W_{soil}, \qquad \textbf{(Equation 1)}$$

where rates are in units tons km^{-2} y^{-1}. If soil thickness (h) is constant over time, then the rate of soil mass loss equals the rate of soil production:

$$\begin{aligned} &if\ \frac{\partial h}{\partial t} = 0, \\ &P_{soil} = E + W_{soil} \end{aligned} \quad . \qquad \textbf{(Equation 2)}$$

Riebe et al. (2003) developed a method to calculate chemical weathering rates in actively eroding terrains by coupling a mass balance approach using immobile elements in weathered residuum (Brimhall and Dietrich, 1987) to rates of landscape lowering derived from cosmogenic radionuclides (CRNs). Fractional enrichment of an immobile element in parent material and the weathered product can be used to calculate relative mass loss due to chemical weathering. Riebe (2001) termed this the chemical depletion fraction (CDF). Using zirconium as the conservative element, the CDF is calculated as:

$$CDF = \left(1 - \frac{[Zr]_p}{[Zr]_w}\right). \qquad \textbf{(Equation 3)}$$

Where the subscript 'p' reflects the parent material concentration and 'w' denotes the concentration in the weathered product. The chemical depletion fraction due to soil weathering (soil relative to saprolite), saprolite weathering (saprolite relative to rock), or total weathering processes (soil relative to rock) can be calculated. We term these respective depletions fractions CDF_{soil}, $CDF_{saprolite}$ and CDF_{total}.

Soil weathering from equation 2 can then be calculated as the product of the soil production rate and the fraction of this rate due to chemical processes:

$$W_{soil} = P_{soil} * \left(1 - \frac{[Zr]_{saprolite}}{[Zr]_{soil}}\right) = P_{soil} * CDF_{soil}. \qquad \textbf{(Equation 4)}$$

The Erosion rate (E) is the difference between soil production and weathering rates:

$$E = P_{soil} - W_{soil}. \qquad \textbf{(Equation 5)}$$

Assuming all regolith, including soil and saprolite, displays a local steady-state thickness over timescales of production, then the saprolite weathering rate is:

$$W_{sap} = P_{soil} * \left(\frac{[Zr]_{saprolite}}{[Zr]_{rock}} - 1\right). \qquad \textbf{(Equation 6)}$$

It is important to note that equations (4-5) differ from ones presented by Riebe et al (2003) in the assumption that CRN derived rates reflect soil production, and not total denudation in regions mantled by saprolite.

Sampling and Laboratory Methodology

Saprolite and soil were sampled at various depths for trace element chemistry. Unweathered bedrock was sampled where available, from beneath soil pits or from outcropping tors. One to three inches of the outside of the sampled rock were removed by rock saw to avoid weathering rinds. All samples were oven dried at 115°C for 48 hours, and homogenized by pulverizing in a tungsten carbide mill to less than 250 μm. Approximately 40g of pulverized material was subsampled for XRF analysis. We

pulverized sample before subsampling in order to obtain as representative a bulk sample as possible, and avoid bias due to oversampling of fines or gravels. Zirconium concentrations in rock, saprolite and soil were measured by pressed pellet XRF at Keene State University (Keene, NH) and ALS-CHEMEX (Reno, NV). These data are used in conjunction with equations presented above to calculate the total CDF, soil CDF, saprolite CDF, soil weathering, saprolite weathering, and physical erosion rates (Table DR 2).

4. Fallout Radionuclides ^{210}Pb and ^{137}Cs and Diffusion-Like Soil Mixing

Sampling and Laboratory Methodology

Soil profiles were sampled at a 2 cm resolution from the surface to the soil/saprolite interface by carefully removing the soil layer by layer with a spatula from a 15x15 cm^2 area. Samples were oven dried at 115°C for 48 hours to remove moisture, and dry sieved with a 2 mm mesh. Soil fines (<2 mm) were then packed into a container of known volume and geometry, and the activity of short-lived radionuclides was measured by gamma ray spectroscopy. Data for activity profiles are provided in Table DR 3. Nuclide inventory is measured in Becquerels/cm^2 as the depth weighted sum of nuclide activity. Within some soils, we additionally sampled at low resolution (5-10 cm) and used these samples to measure bulk soil inventory. Inventory measurements are provided in Table DR 5.

Transport processes and Relevant Timescales

Steady state profiles of ^{210}Pb provide insight into mixing and soil transport over short timescales (10^2-10^3 years). The depth distribution of ^{210}Pb in soils can be described by the steady-state solution to the advection-diffusion equation (e.g., He and Walling, 1997; Kaste et al., 2007):

$$A(z) = A_0 * \exp\left[\frac{V - \sqrt{V^2 + 4\lambda D}}{2D}(z)\right].$$

Where '*A(z)*', is the nuclide activity at a specific depth (in Bq cm^{-3}), 'A_0' is the activity at the surface, 'V' is the downward advection velocity due to leaching (cm y^{-1}), 'λ' is radioactive decay (y^{-1}), and '*D*' is a diffusion like mixing coefficient (cm^2 y^{-1}). Advection rates have previously been measured using the depth of concentration of weapons-derived ^{137}Cs, which was delivered to soils as a thermonuclear bomb product between 1950 and 1970, peaking in 1964 (e.g., Kaste et al., 2007). We were unable to determine clear subsurface peaks in ^{137}Cs activity profiles that correspond to this delivery. Instead, we calculated diffusion-like mixing coefficients by assuming advection plays a minimal role in subsurface nuclide redistribution. Nuclide activity profiles were converted to percent-inventory profiles by dividing activity at depth by the measured inventory for that pit. We then modeled a best fit diffusion equation to each profile by minimizing the sum of residuals. Figure DR 3 shows measured profiles and best-fit models for each site.

Table DR 1: ^{10}Be derived Soil Production Rates

Sample Name	^{10}Be Concentration (atoms g^{-1}) [1]			Sample Depth (cm)	Depth Shielding Factor	Topo Shielding Factor	Soil Production Rate (t km^{-2} yr^{-1})		
Blasingame (36.96° latitude, 220 m elevation at crest)									
BG-0	187403	±	34399	6	0.96	1.00	66.2	±	14.4
BG-1	90282	±	3745	25	0.80	0.99	126.4	±	9.9
BG-2	107038	±	7076	27	0.82	0.99	104.9	±	10.1
BG-3	132701	±	5745	40	0.70	1.00	69.2	±	5.5
BG-4	93307	±	2265	45	0.67	1.00	93.3	±	6.4
BG-5	136789	±	4587	53	0.62	1.00	59.8	±	4.4
BG-6	131622	±	5941	75	0.51	0.99	51.2	±	4.2
White Bark (37.28° latitude, 2991 m elevation at crest)									
WB-0	581657	±	17376	53	0.61	1.00	70.5	±	6.0
WB-1	578575	±	48527	64	0.55	1.00	65.1	±	7.6
WB-2	801896	±	32260	70	0.52	1.00	34.2	±	3.1
WB-3	367081	±	13488	110	0.35	1.00	66.1	±	5.8
WB-4	824462	±	19688	75	0.49	1.00	40.2	±	3.4
WB-5	688245	±	18081	75	0.50	1.00	48.7	±	4.1
WB-6	1081770	±	25628	60	0.57	0.99	35.0	±	3.0
WB-7	406837	±	13257	90	0.43	0.98	71.4	±	6.1
WB-8	789064	±	30516	80	0.47	1.00	40.0	±	3.6

[1] Samples for cosmogenic analysis were processed at Dartmouth College to isolate the beryllium fraction in quartz and then run on an accelerator mass spectrometer at Lawrence Livermore National Laboratory (LLNL) and Purdue Prime Laboratory to determine concentrations of ^{10}Be. We used a production rate of 5.1 atoms ^{10}Be/g quartz/yr and scaled ^{10}Be concentrations for soil depth, slope, topographic shielding, latitude and altitude (Dunne et al., 1999; Gosse and Phillips, 2001; Lal, 1991).

Table DR 2: Chemical Weathering and Erosion

Sample Name	Soil Depth (cm)	Curvature (m^{-1}) [1]	Slope (°)	[Zr] soil (ppm)	[Zr] sap (ppm)	CDF soil	CDF Sap[2]	CDF total[2]	W_{soil} (t km^{-2} y^{-1})	W_{sap} (t km^{-2} y^{-1})	E (t km^{-2} y^{-1})
Blasingame (220 m elev; 36 cm; 16.6 °C)[3]											
LD-0	6	-0.030	1.4	120	130	0.00	0.53	0.50	0.0	75.4	66.2
LD-1	25	-0.027	15.4	103	111	0.00	0.45	0.41	0.0	104.8	126.4
LD-2	27	-0.005	18.5	105	81	0.23	0.25	0.42	24.4	34.4	80.5
LD-3	40	-0.005	15.9	129	64	0.50	0.05	0.53	34.9	3.8	34.3
LD-4	45	0.002	10.1	134	79	0.41	0.23	0.55	38.5	27.5	54.8
LD-5	53	-0.019	6.4	130	81	0.38	0.25	0.53	22.7	19.7	37.1
LD-6	75	-0.012	2.6	139	124	0.11	0.51	0.56	5.5	53.4	45.7
Mean	*39*	*-0.014*	*10.1*	*123*	*96*	*0.23*	*0.32*	*0.50*	*18.0*	*45.6*	*63.6*
Std err	*8*	*0.005*	*2.6*	*5*	*10*	*0.08*	*0.07*	*0.02*	*6.1*	*13.2*	*12.1*
Whitebark (2991 m elev; 107 cm; 3.9 °C)[3]											
WB-0	53	0.000	0.8	182	148	0.18	0.36	0.48	13.0	39.5	57.5
WB-1	64	-0.002	3.6	185	154	0.17	0.38	0.49	10.9	40.7	54.2
WB-2	70	-0.005	6.4	168	215	0.00	0.56	0.43	0.0	43.1	34.2
WB-3	110	0.000	7.1	180	95	0.47	0.00	0.47	31.3	0.0	34.8
WB-4	75	-0.009	9.5	178	155	0.13	0.39	0.47	5.1	25.4	35.1
WB-5	75	-0.004	13.1	223	126	0.44	0.25	0.57	21.2	15.9	27.5
WB-6	60	-0.005	18.8	166	112	0.32	0.15	0.43	11.4	6.4	23.6
WB-7	90	0.000	15.1	234	142	0.40	0.33	0.59	28.3	35.1	43.2
WB-8	80	0.006	7.8	160	138	0.14	0.31	0.41	5.7	18.0	34.3
Mean	*75*	*-0.002*	*9.1*	*186*	*143*	*0.25*	*0.30*	*0.48*	*14.1*	*24.9*	*38.3*
Std err	*6*	*0.001*	*1.9*	*9*	*11*	*0.05*	*0.05*	*0.02*	*3.6*	*5.3*	*3.8*

[1]Curvature measured as the laplacian of elevation from 8m gridded LiDAR data; slope measured from 2m gridded LiDAR data.
[2]Sap CDF and Total CDF calculated using measured zirconium concentrations in rock of 61 ppm at BG and 95 ppm at WB.
[3]Study site (elevation at hillcrest; avg. annual precipitation; avg. annual temperature). Climate data from PRISM online database (Prism-Database).

Table DR 3: BG Fallout Radionuclide Profiles

Sample Depth[1]	^{137}Cs Bq/mm^3	^{137}Cs % Inv [2]	^{137}Cs Cum % [3]	^{210}Pb Bq/mm^3	^{210}Pb % Inv [2]	^{210}Pb Cum % [3]
BG-0-1						
1	7.50	11	11	28.86	23	23
3	8.34	12	24	33.23	27	51
5	12.38	19	42	29.65	24	75
7	12.75	19	61	4.17	3	78
9	7.10	11	72	13.47	11	89
11	8.41	13	85	8.92	7	96
13	7.43	11	96	0.00	0	96
15	2.87	4	100	4.59	4	100
17	0.00	0	100	0.00	0	100
BG-0-2						
1	7.42	15	15	17.67	44	44
3	7.93	16	31	11.85	29	73
5	10.66	21	52	5.32	13	87
7	7.96	16	68	0.00	0	87
9	6.01	12	80	0.97	2	89
11	4.46	9	89	4.45	11	100
13	3.38	7	95	0.00	0	100
15	2.38	5	100	0.00	0	100
17	0.00	0	100	0.00	0	100
BG-1						
1	6.49	11	11	13.97	37	37
3	5.97	10	21	5.26	14	51
5	7.23	12	34	5.83	15	66
7	6.97	12	45	7.17	19	85
9	7.52	13	58	2.04	5	91
11	5.55	9	68	3.08	8	99
13	4.27	7	75	0.00	0	99
15	2.85	5	80	0.41	1	100
17	4.03	7	87	0.00	0	100
19	4.18	7	94	0.00	0	100
21	1.91	3	97	0.00	0	100
23	0.80	1	98	0.00	0	100
25	0.01	0	98	0.00	0	100
27	0.13	0	99	0.00	0	100
29	0.50	1	100	0.00	0	100
31	0.27	0	100	0.00	0	100
21	1.91	3	97	0.00	0	100
23	0.80	1	98	0.00	0	100
25	0.01	0	98	0.00	0	100
27	0.13	0	99	0.00	0	100
29	0.50	1	100	0.00	0	100

Sample Depth[1]	^{137}Cs Bq/mm^3	^{137}Cs % Inv [2]	^{137}Cs Cum % [3]	^{210}Pb Bq/mm^3	^{210}Pb % Inv [2]	^{210}Pb Cum % [3]
BG-2						
1	8.27	16	16	51.98	53	53
3	11.90	22	38	32.06	32	85
5	6.32	12	50	12.28	12	97
7	3.22	6	56	0.68	1	98
9	2.90	5	61	0.00	0	98
11	2.15	4	65	0.00	0	98
13	2.46	5	70	0.00	0	98
15	5.89	11	81	0.00	0	98
17	1.50	3	84	0.00	0	98
19	3.76	7	91	0.00	0	98
21	2.51	5	95	0.00	0	98
23	1.47	3	98	0.00	0	98
25	0.97	2	100	0.00	0	98
27	0.00	0	100	0.00	0	98
29	0.00	0	100	0.97	1	99
31	0.00	0	100	0.97	1	100
BG-4						
1	6.81	17	17	13.46	30	30
3	8.62	22	39	12.70	29	59
5	10.17	26	65	15.18	34	93
7	6.49	17	82	3.00	7	100
10	4.55	12	93	0.00	0	100
12	1.50	4	97	0.00	0	100
14	1.00	3	100	0.00	0	100
17	0.08	0	100	0.00	0	100
19	0.00	0	100	0.00	0	100
21	0.00	0	100	0.00	0	100
BG-5						
1	7.21	11	11	43.26	50	50
3	17.75	28	39	28.92	33	84
5	13.02	20	59	10.55	12	96
7	9.74	15	75	0.00	0	96
9	6.46	10	85	1.96	2	98
11	4.20	7	91	0.00	0	98
13	1.94	3	94	0.00	0	98
15	2.55	4	98	1.76	2	100
17	0.00	0	98	0.00	0	100
19	0.00	0	98	0.00	0	100
21	0.40	1	99	0.00	0	100
23	0.63	1	100	0.00	0	100
25	0.00	0	100	0.00	0	100

Table DR 4: WB Fallout Radionuclide Profiles

Sample Depth [1]	^{137}Cs Bq/mm^3	^{137}Cs % Inv [2]	^{137}Cs Cum % [3]	^{210}Pb Bq/mm^3	^{210}Pb % Inv [2]	^{210}Pb Cum % [3]
WB-0						
1	20.69	38	38	162.04	86	86
3	18.86	34	72	26.88	14	100
5	2.24	4	76	0.00	0	100
7	2.56	5	81	0.00	0	100
9	3.51	6	87	0.00	0	100
11	4.81	9	96	0.00	0	100
13	1.66	3	99	0.00	0	100
15	0.06	0	99	0.00	0	100
17	0.12	0	100	0.00	0	100
19	0.00	0	100	0.00	0	100
21	0.11	0	100	0.00	0	100
23	0.12	0	100	0.00	0	100
25	0.00	0	100	0.00	0	100
27	0.00	0	100	0.00	0	100
29	0.00	0	100	0.00	0	100
31	0.00	0	100	0.00	0	100
WB-2						
1	25.77	29	29	163.80	32	32
	26.38	29	58	154.41	31	63
5	24.69	27	85	168.30	33	96
7	7.71	9	93	19.17	4	100
9	5.67	6	100	0.00	0	100
11	0.21	0	100	0.00	0	100
13	0.00	0	100	0.00	0	100
15	0.00	0		0.00	0	

Sample Depth [1]	^{137}Cs Bq/mm^3	^{137}Cs % Inv [2]	^{137}Cs Cum % [3]	^{210}Pb Bq/mm^3	^{210}Pb % Inv [2]	^{210}Pb Cum % [3]
WB-4						
1	28.13	52	52	71.24	61	61
3	19.37	36	87	46.47	39	100
5	6.82	13	100	0.00	0	100
7	0.03	0	100	0.00	0	100
9	0.00	0	100	0.00	0	100
11	0.00	0	100	0.00	0	100
13	0.00	0	100	0.00	0	100
15	0.00	0	100	0.00	0	100
WB-6						
2	20.45	23	23	115.01	59	59
4	27.98	31	53	37.91	20	79
6	31.34	35	88	41.25	21	100
8	10.13	11	99	0.00	0	100
10	0.75	1	100	0.00	0	100
12	0.00	0	100	0.00	0	100
14	0.00	0	100	0.00	0	100
16	0.00	0	100	0.00	0	100
WB-8						
2	7.65	11	11	51.94	23	23
4	11.34	16	27	102.93	46	69
6	13.27	19	46	69.53	31	100
8	10.45	15	61	0.00	0	100
10	10.50	15	76	0.00	0	100
12	17.02	24	100	0.00	0	100
14	0.00	0	100	0.00	0	100
16	0.00	0	100	0.00	0	100

[1] Average sample depth. Each sample is ~2 cm thick.

[2] Percent inventory measured as ratio of activity to total nuclide inventory.

[3] Cumulative inventory measured as 100%-percent inventory. The depth at which 95% of the inventory is obtained corresponds to the 'Profile Depth' shown in figure 3A of the manuscript.

Table DR 5: Nuclide Inventories

Sample[1]	^{210}Pb Inventory (Bq/m^2)	^{137}Cs Inventory (Bq/m^2)	Upslope Contributing Area (m^2)	Slope (°)
WB-0	3778	1096	0	0.8
WB-2	10114	1808	40	6.4
WB-4	2354	1087	80	9.5
WB-6	3883	1813	120	18.8
WB-8	4488	1405	160	7.8
WB-1 Bulk	9804	2048	20	3.6
WB-2 Bulk	5776	2875	40	6.4
WB-3 Bulk	8540	2776	60	7.1
WB-4 Bulk	6193	2530	80	9.5
WB-8 Bulk	2092	808	160	7.8
BG-0-1	2458	1336	0	1.4
BG-0-2	805	1004	0	1.4
BG-1	755	1174	20	15.4
BG-2	1979	1066	40	18.5
BG-4	887	784	80	10.1
BG-5	1729	1278	100	6.4

[1]Inventories are calculated from profiles shown in Table DR4, and bulk soil samples (noted by 'Bulk').

Table DR 6: Burrowing Activity and Mixing

Transect [1]	Survey Area (m^2)	Burrowing Activity [2] (m^2/km^2)	^{210}Pb 95% Depth [3] (cm)	^{137}Cs 95% Depth [3] (cm)	Mixing Coefficient [3] (cm^2/y)
BG 20m	154	9362	11	21	0.37
BG 60m	162	5983	6	16	0.26
BG 100m	172	4723	5	13	0.13
BG downslope	240	8643	-	-	-
WB 40m	82	3897	5	9	0.19
WB 80m	82	3330	3	5	0.17
WB 120m	82	4906	6	8	0.18
WB downslope	240	3286	-	-	-

[1] Transects at each site include one run downslope from the hillcrest, and three contour-parallel transect at a defined, equally-spaced distance downslope. Hillslope lengths

[2] Burrowing activity calculated as a ratio of the surface area of exposed burrows to the ground area surveyed.

[3] Fallout radionuclide and mixing coefficient data obtained from equivalent downslope pit. These are: BG 20m (BG-1); BG 60m (average BG-2 & BG-4); BG 100m (BG-5); WB 40m (WB-2); WB 80m (WB-4); WB 120m (WB-6).

Figure DR 1:

Image from a soil pit at Blasingame. Note the clear, irregular soil saprolite boundary. It has been actively disrupted by gopher burrowing, a soil production mechanism at this site.

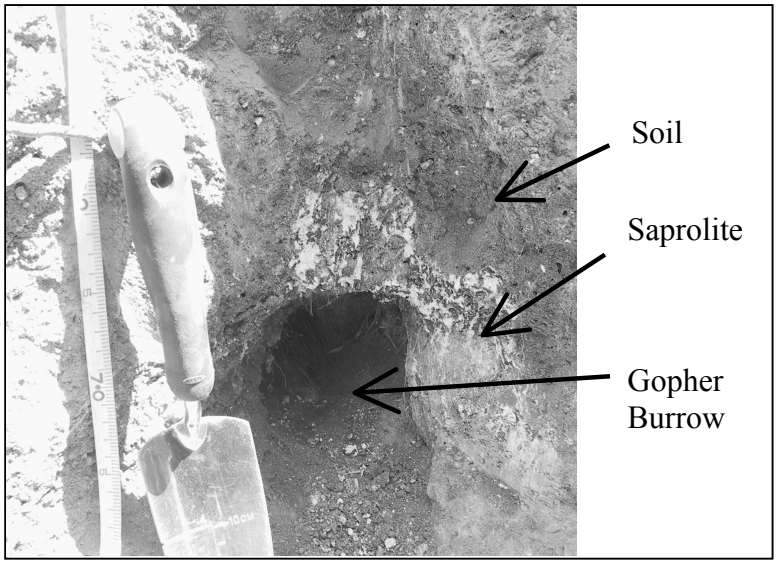

Figure DR 2:

(A,B) Profiles of elevation (black line) and soil depth (grey diamonds) for sampled hillslopes. (C,D) Topographic map of study sites and surrounding hillslopes. DEM from 1 m gridded Lidar provided by NCALM. Lines represent 20 m elevation contours. (E,F) Photos at each site. BG photo taken looking south from an adjacent hillcrest and WB photo taken looking downtransect (SW) from WB hillcrest.

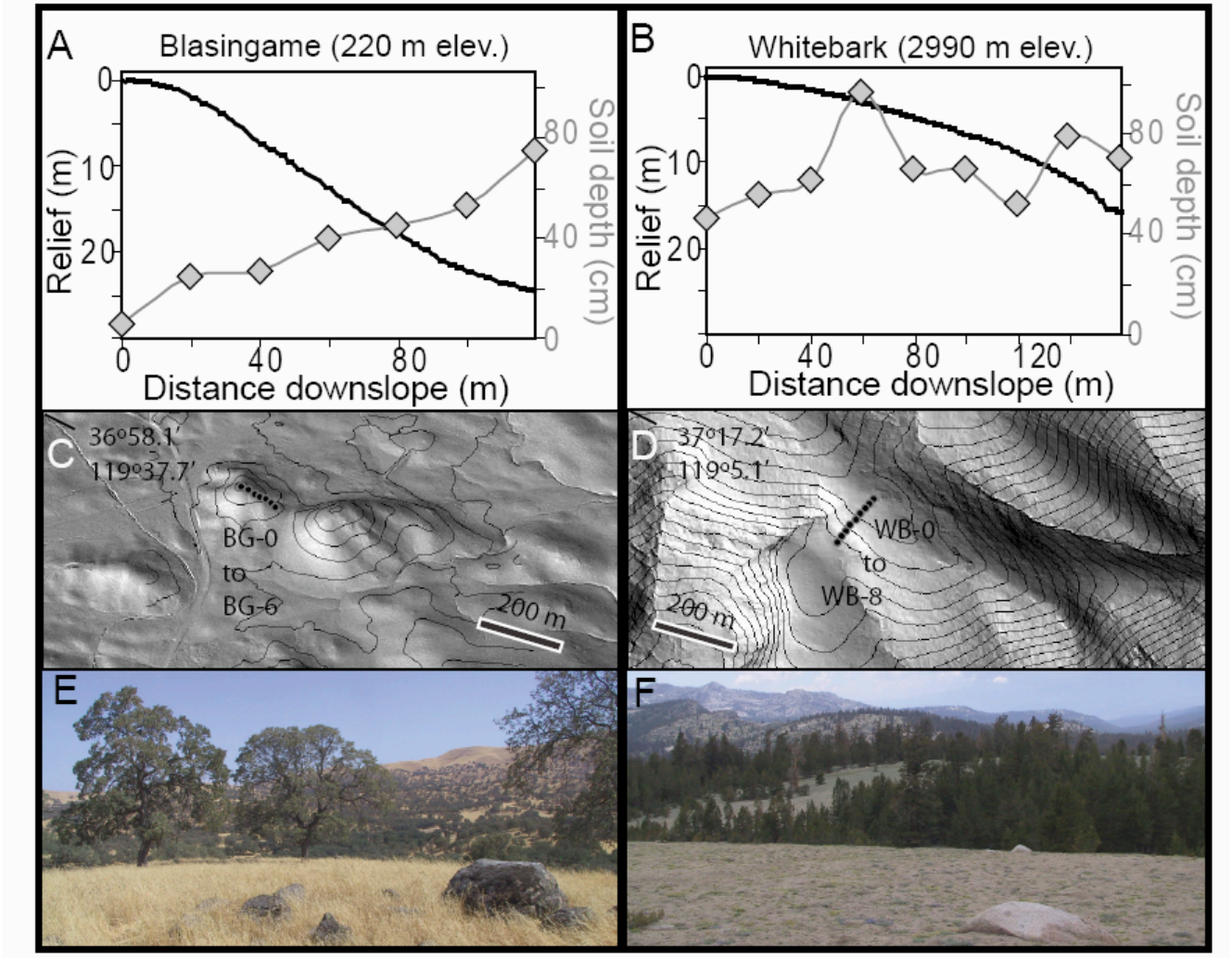

Figure DR 3:

Downslope activity profiles of ^{210}Pb show distinct patterns at elevation extremes, especially at hillcrests. Coefficients of Diffusion were calculated following model of Kaste et al, (2007), however in this study we assume down profile advection is minimal. Profile data is shown by black circles with error bars. Modeled best-fit diffusion profiles are shown with grey line. Two profiles were captured at one low elevation hillcrest BG-0 (~2m apart).

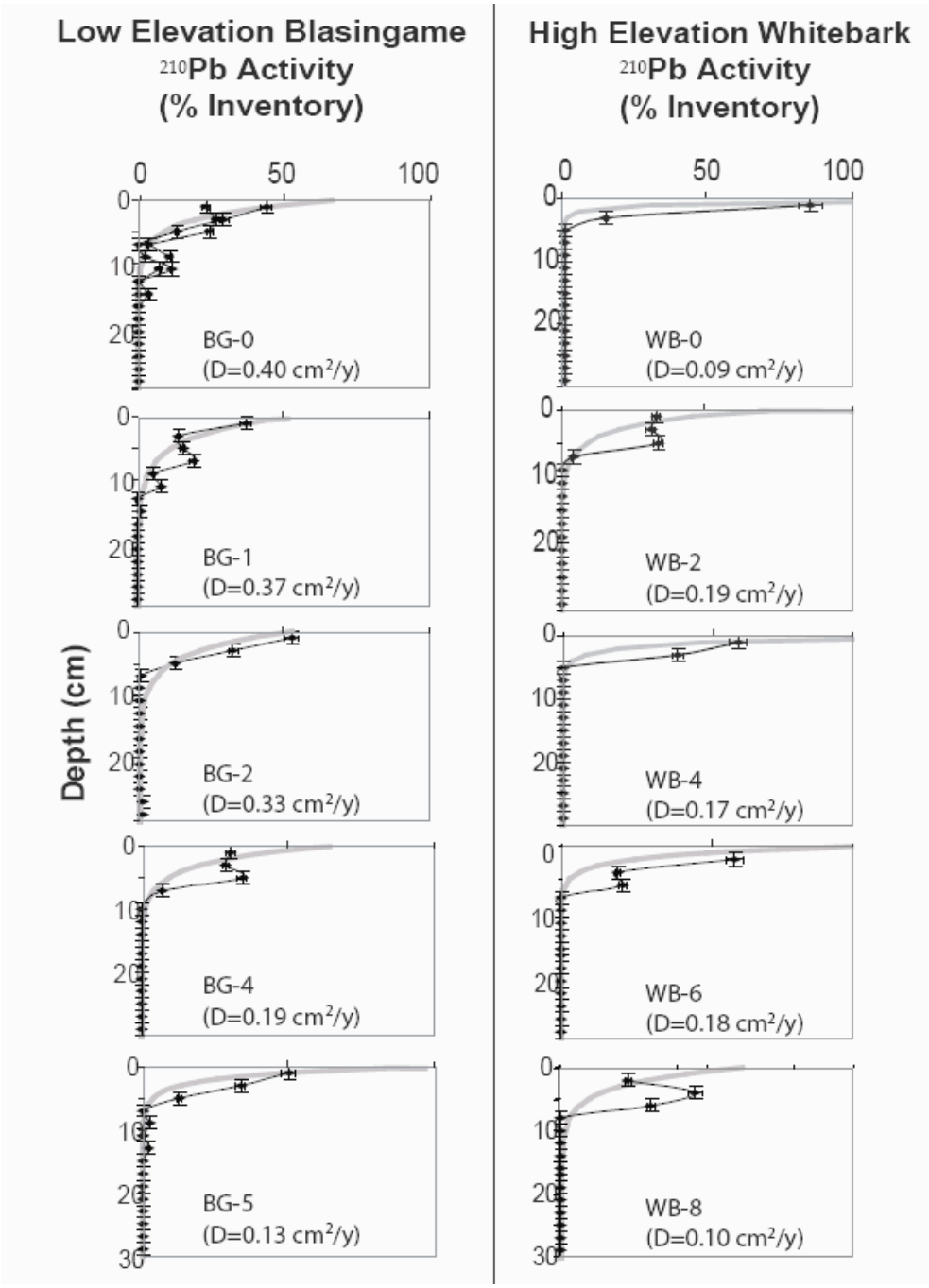

REFERENCES CITED

Balco, G., Stone, J.O., Lifton, N.A., and Dunai, T.J., 2008, A complete and easily accessible means of calculating surface exposure ages or erosion rates from 10Be and 26Al measurements: Quaternary Geochronology, v. 3, p. 174.

Black, T.A., and Montgomery, D.R., 1991, Sediment transport by burrowing animals, Marin County, California: Earth Surface Processes and Landforms, v. 16, p. 163-172.

Brimhall, G.H., and Dietrich, W.E., 1987, Constitutive mass balance relations between chemical composition, volume, density, porosity, and strain in metasomatic hydrochemical systems: Results on weathering and pedogenesis: Geochimica et Cosmochimica Acta, v. 51, p. 567.

Dunne, J., Elmore, D., and Muzikar, P., 1999, Scaling factors for the rates of production of cosmogenic nuclides for geometric shielding and attenuation at depth on sloped surfaces: Geomorphology, v. 27, p. 3-11.

Gosse, J.C., and Phillips, F.M., 2001, Terrestrial in situ cosmogenic nuclides: theory and application: Quaternary Science Reviews, v. 20, p. 1475-1560.

He, Q., and Walling, D.E., 1997, The distribution of fallout Cs-137 and Pb-210 in undisturbed and cultivated soils: Applied Radiation And Isotopes, v. 48, p. 677-690.

Heimsath, A.M., Dietrich, W.E., Nishiizumi, K., and Finkel, R.C., 1999, Cosmogenic nuclides, topography, and the spatial variation of soil depth: Geomorphology, v. 27, p. 151-172.

Kaste, J.M., Heimsath, A.M., and Bostick, B.C., 2007, Short-term soil mixing quantified with fallout radionuclides: Geology, v. 35, p. 243-246.

Kaste, J.M., Heimsath, A.M., and Bostick, B.C., 2007, Short-term soil mixing quantified with fallout radionuclides: Geology, v. 35, p. 243-246.

Lal, D., 1991, Cosmic ray labeling of erosion surfaces: in situ nuclide production rates and erosion models: Earth and Planetary Science Letters, v. 104, p. 424-439.

Prism-Database, http://www.prismclimate.org, created 5 Mar 2008, PRISM Group, Oregon State University

Riebe, C.S., Kirchner, J.W., and Finkel, R.C., 2003, Long-term rates of chemical weathering and physical erosion from cosmogenic nuclides and geochemical mass balance: Geochimica et Cosmochimica Acta, v. 67, p. 4411-4427.

Riebe, C.S., Kirchner, J.W., Granger, D.E., and Finkel, R.C., 2001, Strong tectonic and weak climatic control of long-term chemical weathering rates: Geology, v. 29, p. 511-514.